BLUR IDENTIFICATION IN SATELLITE IMAGERY USING AN IMAGE DOUBLET

Timo Rolf Bretschneider

Assistant Professor, School of Computer Engineering
Nanyang Technological University
Blk. N4 #02a-32, Nanyang Avenue, Singapore 639798
Tel: +65 – 6790 – 6045 Fax: +65 – 6792 – 6559
E-mail: astimo@ntu.edu.sg
SINGAPORE

KEY WORDS: point spread function, image doublets, blurring estimation

ABSTRACT:

Knowledge of the point spread function (PSF) for a given image acquisition system is of fundamental importance since it enables an objective assessment of the imaging performance. Moreover it allows the utilisation of image restoration techniques for posterior image improvement. Pre-flight measurements and calibrations using an optical bench partly make a better understanding about the imaging system possible but are expensive – particularly in cases with a limited budget like for example mini-satellite missions or where the opportunity to undergo rigorous testing procedures on the flight-model are limited. However, there are cheaper alternatives, which even can be utilised after launch with the additional advantage of providing a tool to monitor possible instrument degradations. Several scanners provide modes for obtaining imagery of the same scene with different spatial resolution. These images can be used to solve for the unknown imaging function, whereby the more highly resolved scene is used as an estimate of the unblurred version of the less highly resolved data, with the PSF itself estimated using deconvolution techniques. This paper investigates different algorithms and analyses the inherent critical assumptions if image doublets with different spatial and spectral characteristic are employed. Examples will be shown for a scanner called MOMS, which provides a typical example for the attainable performance of imaging systems in the midrange multispectral resolution.

1. INTRODUCTION

An important element for the characterisation of a satellite's performance is the point spread function (PSF). Furthermore the function can be used in image restoration to improve the spatial resolution and in image analysis, e.g. to locate certain image features to sub-pixel accuracy. The estimation of the imaging function is often not straightforward since the electro-optical systems used in nowadays satellites consist of a number of components, each with properties that may not be precisely characterised or which exhibit changing characteristics. Pre-flight measurements and calibrations using an optical bench partly allow gaining a better understanding about the imaging system. Unfortunately many of the upcoming small satellite missions do not permit the involved costs since the highly specialised manpower and the required optical facilities are expensive. Moreover the actual flight model often cannot be exposed to the same rigorous test procedures like the evaluation model to minimise undesired ageing, contamination etc.

However, several scanners provide imagery with different spatial resolution of the same scene, which can be either obtained simultaneously or within a short period in time. A minimisation of the time delay between the acquisitions of the corresponding image sets is considered necessary to reduce the impact of distortions from changed viewing conditions etc. The differently resolved images can be used to solve for the unknown imaging function whereby the more highly resolved scene is used as an estimate of the unblurred version of the less highly resolved data, with the PSF itself estimated using deconvolution techniques. The paper investigates two different approaches, namely the Wiener filter and the maximum likelihood estimation, whereby both are implemented iteratively to support additional constraints on the solution. The approach relies on a number of assumptions (McNeill and Pairman, 1998). First, the spectral response is assumed to be nearly the same between the two different image sets. This holds true for some cases, e.g. with respect to the panchromatic and the second multispectral band of SPOT-4, but generally can only be approximated by a weighted sum of the typically lower resolved multispectral bands. The second inherent assumption requires that the corresponding instruments should have the same spatial frequency characteristic. Third the spatial frequency energy

of the more highly resolved image must extend far beyond the sampling interval of the more coarsely given imagery to enable a reasonable estimate.

As an example for the capabilities of the proposed method images from a scanner called MOMS were chosen. The system flew in different configurations onboard of Space Shuttle missions and the MIR Space Station. Although the design does not reflect the state-of-the-art with respect to nowadays high-end scanners it provides a reasonable illustration since many upcoming mini- and small-satellite mission of space emerging counties will provide comparable imaging facilities. In case of solely multispectral acquisition abilities a more highly resolved image from an airborne camera has to be used for the validation of the satellite's scanner performance.

2. IMAGE DEGRADATION PROCESS AND IMAGE-BASED BLURRING ESTIMATION METHODS

The linear space-invariant image degradation process can be modelled (Bates and McDonnell, 1986) by

$$g(x, y) = \int_{-\infty}^{\infty}\int_{-\infty}^{\infty} f(x', y')h(x - x', y - y')\,dx'dy' + n(x, y) \tag{1}$$

where g is the blurred image, f the observed object, h the space-invariant PSF itself, and n the uncorrelated additive noise. The pair (x,y) represents the location in the continuous two-dimensional space. However, in practice the functions are sampled at discrete locations and the integral on the right hand side of Equation (1) becomes a summation. Therefore the equation can be rewritten as

$$g(x, y) = f(x, y) * h(x, y) + n(x, y), \tag{2}$$

where the operator $*$ represents 2-dimensional convolution. Imaging systems are seldom truly space-invariant, but Equation (2) usually holds true within a limited region of a measured image. The transformation of the equation into the Fourier domain leads to

$$G(u,v) = F(u,v)H(u,v) + N(u,v), \tag{3}$$

where G, F, H, and N are the Fourier transforms of the corresponding lower case variables and the pair (u,v) represents the location in the spatial frequency domain. The convolution becomes a point-wise multiplication of the object spectrum with the optical transfer function (OTF) H. The modulation transfer function (MTF) is the magnitude of H and, by assuming a zero phase, i.e. an aberration free system, an estimate of the PSF can be obtained by the inverse Fourier transformation of the MTF.

Deconvolution techniques invert the impact of the PSF and enable the computation of more highly resolved images. Equivalently inverse filtering techniques compensate for the influence of the MTF in the Fourier domain. Henceforth both domains will be used synonymous since for every algorithm in one domain there is an equivalent in the other domain. For a reliable deconvolution precise knowledge about the noise model, the PSF, and / or some constraints with respect to the solution space are required. In the first case special estimation techniques (Gao, 1993), (Rank et al., 1999) can be utilised. However, the estimation of the imaging function in the second case is often not straightforward since the image acquisition system consists of a number of components, each with properties that may not be precisely characterised or which exhibit changing characteristics. Papers dealing with the task of estimating the PSF can be grouped into theoretical approaches, direct pre-flight measurements of the instrument characteristics, and techniques for the estimation of the blurring function from images. A more detailed overview about the three groups with corresponding results related to remote sensing can be found in (Bretschneider et al., 2001). In summary most of the model-based approaches consider only parts of the image acquisition chain and generally suffer from modelling and parameterisation uncertainties. Pre-flight measurements are limited to certain components of the system, too, and like the first group cannot describe any degradation over time. The main advantages of image-based techniques are the low costs, the utilisation even if no direct access to the scanner and its design details is provided, and the monitoring of time dependent aspects. Therefore this paper focuses on this group of estimation techniques. However, the proposed approach extends beyond the often utilised extraction of a small set of profiles over well-known sharp edges and the subsequent parameter estimation assuming that the PSF is closely approximated by a Gaussian distribution (Berger and Kaufmann, 1994). The major drawbacks of the profile technique are the generally required supervision, the problem

of repeatability if no adequate features are contained in the image, and the frequently made simplification that the PSF is radial symmetric.

3. BLUR IDENTIFICATION METHODS

In the following two different iterative approaches are summarised that enable to estimate the PSF h and MTF H in Equation (2) and Equation (3), respectively.

3.1. Wiener Filter

Originally the usage of the Wiener filter was proposed by McNeill and Pairman (McNeill and Pairman, 1998) to estimate the PSF of SPOT using the twin instrument configuration. The almost identically instruments HRV-1 and HRV-2 were used simultaneously to capture an image of the same ground target, with essentially identical viewing geometries (i.e. the same mirror step position), with one instrument in panchromatic mode and the other in multispectral. With the panchromatic band as an estimate of the unblurred version of the multispectral response, at least out to the Nyquist frequency of the multispectral sensor, a modified form of the classical Wiener filter restoration method was used to compute the MTF. Thus

$$\hat{H}(u,v) = \frac{G_P(u,v) \cdot G_M(u,v)}{|G_P(u,v)|^2 + \Phi_N / \Phi_H}, \tag{4}$$

where $\hat{H}(u,v)$ is an estimate of $H(u,v)$, G_P is the spectrum of the more highly resolved panchromatic band image, and G_M the spectrum of the combination of the multispectral bands. A detailed description for the calculation of G_M will be provided in Section 4. The parameters Φ_N and Φ_H in Equation (4) are the power spectra (as functions of spatial frequencies) of the noise and the actual MTF, respectively. If white noise is assumed the corresponding power spectrum Φ_N is uniform. For a more accurate estimate either a noise estimation algorithm (Gao, 1993), (Rank et al., 1999) can measure Φ_N or the equation $\Phi_G = |H|^2 \Phi_F + \Phi_N$ is utilised. Since knowledge about the MTF itself is required in the latter case, this paper suggests an iterative version of Equation (4) to estimate H, i.e.

$$\hat{H}(u,v,k+1) = \frac{G_P(u,v) \cdot G_M(u,v)}{|G_P(u,v)|^2 + \Phi_N / \Phi_{\hat{H}(u,v,k)}}, \tag{5}$$

where k describes the iterative process. For a first estimate of Φ_H the power spectrum is assumed to be constant. Henceforth in this paper the iterative computation will be used since it resulted according to simulations in more accurate PSF estimates.

3.2. Maximum Likelihood

The main idea of the maximum likelihood approach is to minimise the term $g - f * h$, i.e.

$$\frac{\partial}{\partial \hat{h}(x,y)} \sum_{x,y} \left(g - f * \hat{h} \right)^2 = 0, \tag{6}$$

where g and f represent the weighted combination of multispectral bands and the more highly resolved panchromatic band, respectively. The parameter $\hat{h}$ is an estimate of the actual point spread function h. The original iterative implementation of Equation (6) has the two main advantages of non-negativity with respect to the result as well as convergence and is described by

$$\hat{h}_{k+1} = \hat{h}_k \left(f \bullet \frac{g}{(\hat{h}_k * f)} \right), \tag{7}$$

with the operator $\bullet$ indicating correlation. The underlying noise model incorporates the Poisson statistic and therefore is not appropriate for the given problem. Hence, this paper suggests a modification of Equation (7) similar to the idea depicted by Pruksch and Fleischmann (Pruksch and Fleischmann, 1998) to include Gaussian statistics:

$$\hat{h}_{k+1} = \hat{h}_k \left(f \bullet \frac{g}{\left(\hat{h}_k \ast f\right) \bullet f} \right) \tag{8}$$

In case of noisy data a shortcoming is the noise amplification, since the maximum likelihood algorithm tries – according to Equation (6) – to fit the data as closely as possible. One possible solution to avoid this undesired effect is the integration of a damping factor like it is often used in image restoration (White, 1994). However, for the particular case of estimating the PSF the utilisation of constraints on the intermediate estimates within every iteration leads to faster convergences and allows a more flexible approach to include additional a-priori knowledge about the imaging function. This paper utilised the two constraints that the PSF has finite extent and is point-symmetric, which is reasonable with respect to the design of most push-broom scanners.

4. MOMS SCANNER AND DATA

The German MOMS-02P (Modular Optoelectronic Multispectral Stereo-Scanner) is the technical continuation of MOMS-01 and MOMS-02 flown on board of the Russian space station MIR. The push-broom camera consists of a threefold stereoscopic imaging system and a four band multispectral camera with nadir orientation. In this paper imagery obtained in mode C was analysed. The specific mode provides three multispectral bands acquired with two identical objectives having each a focal length of 220 mm and a more highly resolved panchromatic band using a telescope with a focal length of 660 mm. To attain sufficient swath, two coupled Fairchild CCD191 are used in the focal plane of the panchromatic optics while one CCD per band is used for the multispectral data, i.e. two CCD arrays are placed in the focal plane of each 220 mm objective to gain four individual bands in total from which only three bands are supported in mode C. The details for the four bands are shown in Table 1. Note that the values are given with respect to the PRIRODA mission using the MIR space station as platform with an inclination of 51.6° and a mean orbital altitude of 400 km.

Mode	Channel	Pixels per line	Swath	Spectral coverage	GSD
Multispectral	2	3220	57.96 km	532 – 576 nm	18×18 m
	3	3220	57.96 km	645 – 677 nm	18×18 m
	4	3220	57.96 km	772 – 815 nm	18×18 m
Panchromatic	5	6000	36 km	512 – 765 nm	6×6 m

Table 1: Selected performance parameters of the MOMS-02P camera in mode C

The utilised scene for this paper was acquired on the 11th of December 1996 over East Australia and shows mainly agricultural land use with an urban settlement in the centre portion of the scene. Figure 1 depicts two sub-scenes of the panchromatic and multispectral band C_3, respectively, and gives an insight in the imaging capacities. Note that the data is a level 1A product, i.e. no resampling of the original image was performed.

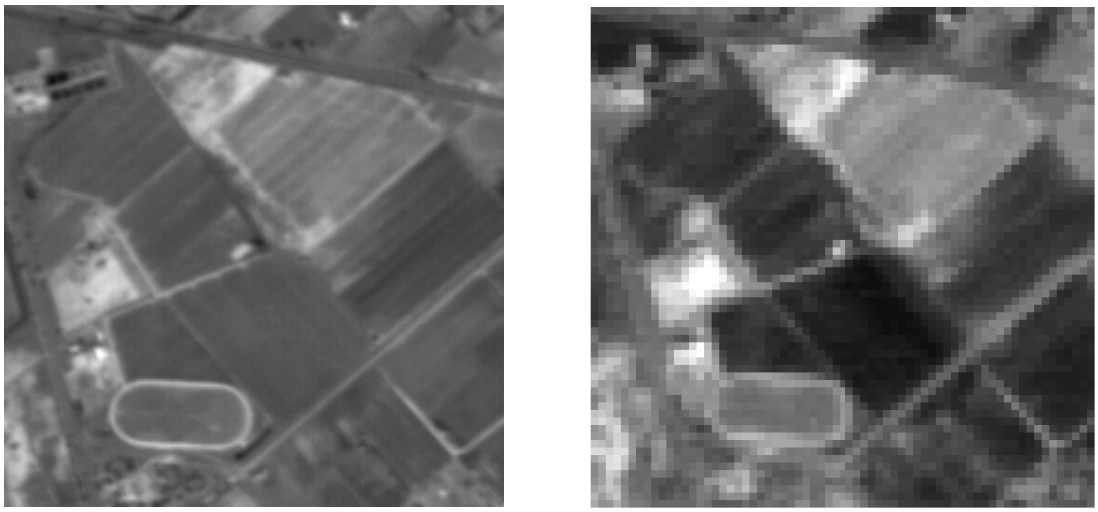

(a) (b)

Figure 1: Sub-images from a scene obtained by MOMS on the PRIRODA mission (contrast enhanced): (a) panchromatic band, (b) multispectral band C_3 resampled to the same size as the panchromatic band

An analysis of the panchromatic scene revealed artefacts in the first 22 columns, i.e. a strong discontinuity between the 22nd and 23rd column. However, the typical striping in panchromatic imagery due to the often used separate readout of odd and even CCD pixel positions was not observed. Also no spectral discontinuities between the two different CCD sensors could be exposed.

It was reported* that the relative locations of the eight CCD arrays with respect to each other might change due to the environmental influences, i.e. the shift amount can change from scene to scene due to physical changes of the centre plate during the mission (Berger and Kaufmann, 1994). This shift was taken into consideration by estimating the displacement (Fonseca and Manjunath, 1996) and subsequently resampling of the mage doublets with respect to the panchromatic band.

According to Section 3 the panchromatic band of the shown MOMS scene in Figure 1 can be used as an estimate of the unblurred version of the less highly resolved data. However, one major requirement for a successful utilisation of the techniques is the spectral alignment between the lower resolved image and the corresponding more highly resolved version. Generally the different bands of a scanner are not spectrally aligned and therefore a weighted sum of the multispectral image set is used to approximate the spectral characteristic of the panchromatic scene. Let MS^R_i be the resampled versions of the corresponding multispectral bands MS_i – the calculation uses a Kaiser-weighted sinc interpolator and resamples with respect to the pixel centres of the more highly resolved data. Then the artificially created band P_{MS} with

$$P_{MS} = \sum_{i=1}^{K} a_i \cdot MS_i^R + b_i \tag{9}$$

represents the panchromatic equivalent to the actual panchromatic band P at the lower spatial resolution but the same number of pixels. The variables K, a_i, and b_i describe the number of bands, a linear scaling factor, and a band-specific offset, respectively. To gain the a_i and b_i Equation (9) can be rewritten in matrix notation by ordering the $N \times M$ image pixels lexicographically according to their row and column indices. Furthermore P_{MS} is replaced by the panchromatic data P to determine the best fit between the weighted multispectral and panchromatic data.

$$\underbrace{\begin{bmatrix} P(1) \\ \vdots \\ P(N \cdot M) \end{bmatrix}}_{P} = \underbrace{\begin{bmatrix} MS_1^R(1) & \cdots & MS_K^R(1) & 1 & \cdots & 1 \\ \vdots & & \vdots & \vdots & & \vdots \\ MS_1^R(N \cdot M) & \cdots & MS_K^R(N \cdot M) & 1 & \cdots & 1 \end{bmatrix}}_{D} \underbrace{\begin{bmatrix} a_1 & \cdots & a_K & b_1 & \cdots & b_K \end{bmatrix}^T}_{Q}. \tag{10}$$

* MOMS user guide. http://www.nz.dlr.de/moms2p/ug/index.html

Note that the problem is over-determined, i.e. D is not squared and therefore the pseudo-inverse $D^{\#}$ defined as

$$D^{\#} = \left(D^T D\right)^{-1} D^T \tag{11}$$

has to be used to solve for the parameters in Q, i.e. $Q=D^{\#}P$. The newly created image P_{MS} is optimal in a least squares sense. The approach should only be used locally for sub-sections of the image to enable a flexible adaptation to the respective reflectance of the displayed ground cover. Consequently the PSF estimation takes place within the given region and should not overlap with other regions, which were generated using a different choice of parameters a_i and b_i. For an analysis on the introduced errors by using a linear combination of multispectral bands to simulate a panchromatic band refer to (Mascarenhas et al., 1991).

5. RESULTS

The comparison between the results of the different methods presented in Section 3 is made using the full-width-half-maximum (FWHM) values of the estimated imaging functions. For both iterative approaches the FWHM values were taken in the across-track and the along-track direction. Since the estimated PSFs are slightly irregular in shape a least squares fitted ellipse was employed to avoid an undesired bias in the measurement. Several different sub-images were used for the estimation process to minimise the influence of local characteristics in the image bands and finally the different estimates averaged. The results are summarised in Table 2 whereby each estimation algorithm utilised one of the two previously mentioned constraints, i.e. compact support or point-symmetry. Note that the values in Table 2 are with respect to the multispectral pixels of the used scene.

The extent of the PSF estimated by the iterative Wiener filter is larger than the maximum likelihood estimate. The reason is that the Wiener filter itself has a low-pass characteristic. However, this is partly compensated by superimposing a finite extent on the intermediate results and thus introducing high frequency components. On the contrary the symmetry constraint broadens the PSF even further and does not limit the extent since earlier – presumable invalid – estimates in the outer skirt are never completely revised. The same argumentation regarding the constraints is applicable for the estimates using the maximum likelihood estimation. However, the differences are less significant. A first analysis (work in progress) between the two different iterative approaches led to the assumption that the results of the maximum likelihood estimator are more likely to describe the actual PSF.

	Wiener Filter		Maximum Likelihood	
	Extent	Symmetry	Extent	Symmetry
$FWHM_{across-track}$	2.63	2.85	2.51	2.63
$FWHM_{along-track}$	2.97	3.07	2.66	2.74

Table 2: FWHM values for the PSF estimates

Further investigations using the proposed techniques have shown that the shape of the estimated PSF is nearly space invariant over the entire image plane. This would be expected for the along-track direction since MOMS is a push-broom scanner. The variation in the across-track direction is negligible due to the narrow instantaneous field of view.

6. CONCLUSIONS

A method for estimating the PSF of a remotely sensed image has been described, relying on the existence of an image doublet with different spatial resolution. The more highly resolved panchromatic image was used as an estimate of the unblurred multispectral image sets. The approach takes into account that the spectral information varies across the different bands but assumes in general a high correlation among corresponding image sections. Two different iterative techniques were depicted to compute the PSF estimate using the idea of Wiener filtering and maximum likelihood deconvolution, respectively.

The main advantage of the proposed technique is that it allows an unsupervised computation of non-radial symmetric PSFs. Therefore the differences of the PSF extent in the along-track and the across-track direction are observable. The approach is solely based on some basic assumptions concerning

the extent of the spatial frequencies beyond the less highly resolve image and the spectral characteristic. While the first constraint generally becomes less prevailing if the difference in spatial resolution between the doublets increases (Viallefont-Robinet and Henry, 2000), the latter one can only be partly compensated by approximating the spectral attributes using a weighted set of multispectral bands.

The foremost drawback of the proposed algorithm is that only the PSF of the less highly resolved image set can be estimated. Furthermore no estimations for individual bands are possible as long as the doublets are not spectrally aligned. However, once the actual shape of the imaging function is computed the PSF can be approximated by a suitable model, which then can compensate for the difference between the bands, i.e. the wavelength dependent diffraction. Future work will consider the extrapolation of the PSF estimate to the panchromatic band.

REFERENCES

Bates, R., McDonnell, M., 1986. Image Restoration and Reconstruction, Clarendon Press.

Berger, M., Kaufmann, H., 1994. Performance verification of spectral and panchromatic modules of the MOMS-02 sensor flown aboard STS-55/D2-mission. IEEE Proceedings of the International Geoscience and Remote Sensing Symposium, 4, pp. 2301–2304.

Bretschneider, T., Bones, P.J., McNeill, S., Pairman, D., 2001. Image-based quality assessment of SPOT data. Proceedings of the American Society for Photogrammetry & Remote Sensing, CD-ROM.

Gao, B.-C., 1993. An operational method for estimating signal to noise ratios from data acquired with imaging spectrometers. Remote Sensing of the Environment, 43, pp. 23–33.

Fonseca, L., Manjunath, B.S., 1996. Registration techniques for multisensor remotely sensed imagery. Photogrammetric Engineering and Remote Sensing, 62(9), pp. 1049–1056.

Mascarenhas, N., Banon, G., Fonseca, L., 1991. Simulation of a panchromatic band by spectral linear combination of multispectral bands. IEEE Proceedings of the Int. Geoscience and Remote Sensing Symposium, 1, pp. 321–324.

Nelder, J.A, Mead, R., 1965. A simplex method for function minimization. Computer Journal, 7, pp. 308–313.

McNeill, S., Pairman, D., 1998. Estimation of the SPOT multispectral sensor point spread function. Proceedings of the 9th Australasian Remote Sensing and Photogrammetry Conference, CD-ROM.

Pruksch, M. Fleischmann, F., 1998. Positive iterative deconvolution in comparison to Richardson-Lucy like algorithms. Proceedings of the Astronomical Society Conference Series, 145, pp. 469–499.

Rank, K Lendl, M., Unbehauen, R., 1999. Estimation of image noise variance. IEE Proceedings on Visual Image Signal Processing, 146(2), pp. 80–84.

Viallefont-Robinet, F., Henry, P., 2000. VEGETATION MTF in-flight measurement using HRVIR. Proceeding of the SPIE - Earth Observing Systems V, 4135, 314–323.

White, R.L., 1994. Image restoration using the damped Richardson-Lucy method. Proceedings of the Workshop of Restoration of HST Images and Spectra – II, pp. 104–110.